Supplementary Information (SI) for RSC Applied Interfaces.
This journal is © The Royal Society of Chemistry 2026

Electronic Supporting Information for

Dual-Function Catalysis: Linking Photo- and Electrocatalytic Behavior in In_2O_3/TiO_2 Composites

Hanna Maltanava, Nikita Belko, Pauliina Nevalainen, Niko M. Kinnunen,
Konstantin Tamarov, Jani O. Moilanen, Jari T.T. Leskinen, Vesa-Pekka Lehto, Polina Kuzhir

Contents

1. Additional characterization data

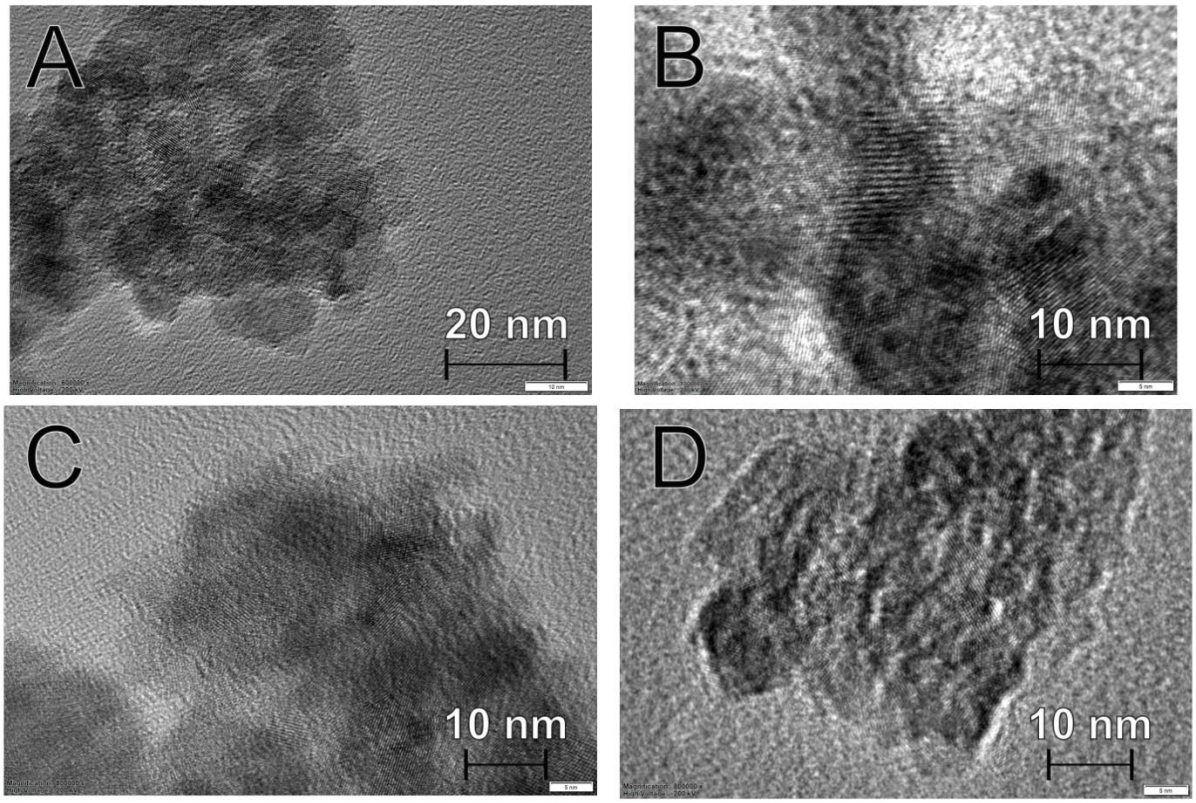

Fig. S1. High resolution TEM micrographs of the prepared oxide powders: TiO_2-300 (A), In_2O_3-300 (B), In_2O_3/TiO_2(30)-300 (C), and In_2O_3/TiO_2(90)-300 (D).

Table S1. Assignment of XRD reflexes for TiO_2 powder annealed at 600 °C.

#	**Measured 2ϑ (°)**	**Database 2ϑ (°)**	**Phase**	***hkl* indices**
1	25.12	25.34	anatase	1 0 1
2	27.26	27.24	rutile	1 1 0
3	30.7	30.86	brookite	1 2 1
4	35.9	35.80	rutile	1 0 1
5	37.59	37.80	anatase	0 0 4
6	39.02	38.92	rutile	2 0 0
7	41.07	40.92	rutile	1 1 1
8	43.87	43.72	rutile	2 1 0
9	47.88	48.10	anatase	2 0 0
10	54.16	53.90	rutile	2 1 1
11	56.46	56.20	rutile	2 2 0

Table S2. Assignment of XRD reflexes for In_2O_3 powder annealed at 300 ºC.

#	**Measured 2*ϑ* (º)**	**Database 2*ϑ* (º)**	**Phase**	***hkl* indices**
1	21.50	21.50	cubic In_2O_3	2 1 1
2	30.58	30.58	cubic In_2O_3	2 2 2
3	35.45	35.46	cubic In_2O_3	4 0 0
4	37.74	37.70	cubic In_2O_3	4 1 1
5	39.84	39.82	cubic In_2O_3	2 4 0 / 4 2 0
6	41.84	41.84	cubic In_2O_3	3 3 2
7	43.78	43.80	cubic In_2O_3	4 2 2
8	45.68	45.68	cubic In_2O_3	3 4 1 / 4 3 1
9	49.32	49.30	cubic In_2O_3	2 5 1 / 5 2 1
10	51.04	51.02	cubic In_2O_3	4 4 0
11	52.76	52.72	cubic In_2O_3	4 3 3
12	54.32	54.36	cubic In_2O_3	4 4 2 / 6 0 0
13	55.94	55.98	cubic In_2O_3	3 5 2 / 6 1 1 / 5 3 2
14	57.65	57.58	cubic In_2O_3	2 6 0 / 6 2 0
15	59.21	59.14	cubic In_2O_3	4 5 1 / 5 4 1

2. Additional photocatalytic data

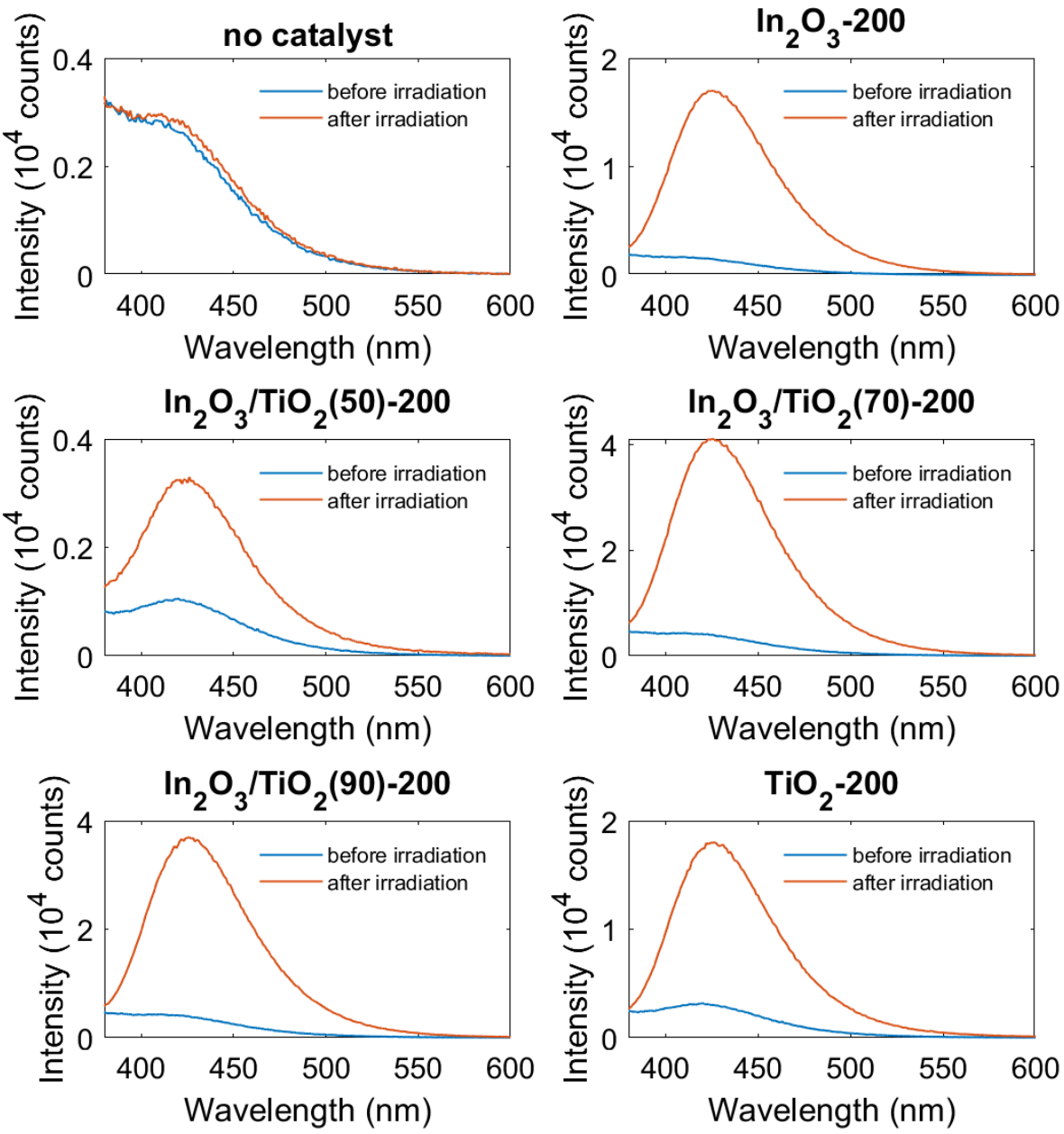

Fig. S2. Fluorescence spectra of the oxidation product of terephthalic acid (2-hydroxyterephthlic acid) generated in suspensions of In_2O_3, TiO_2, and In_2O_3/TiO_2 powders annealed at 200 °C after irradiation at 385 nm with a light dose of 36 J cm^{-2}.

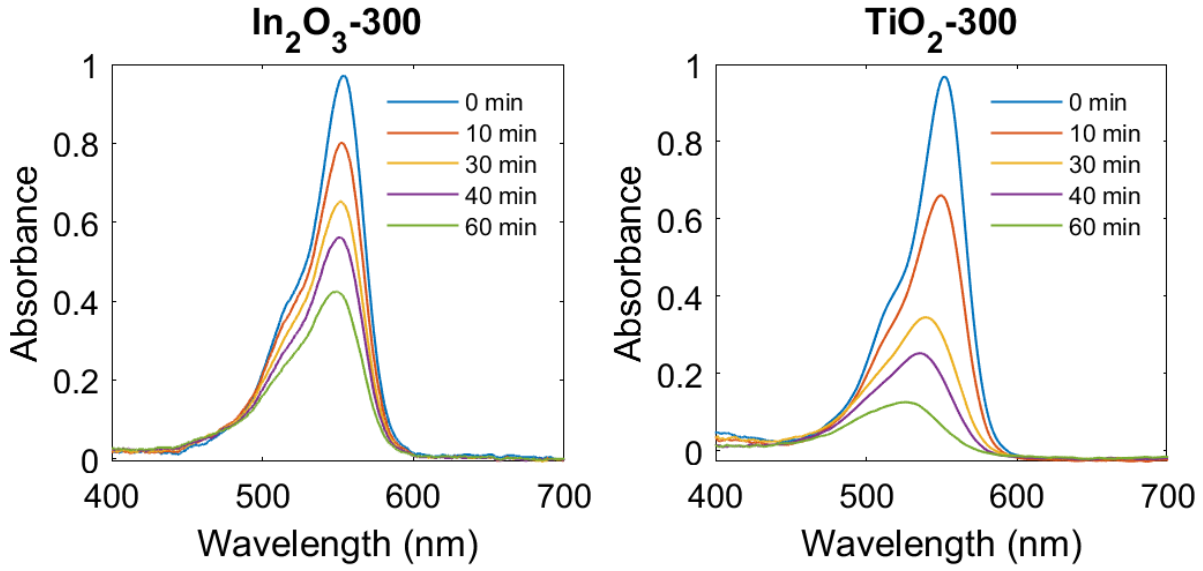

Fig. S3. Absorption spectra of RhB before and after irradiation (365 nm, 150 mW cm^{-2}) in the presence of In_2O_3 and TiO_2 powders annealed at 300 °C.

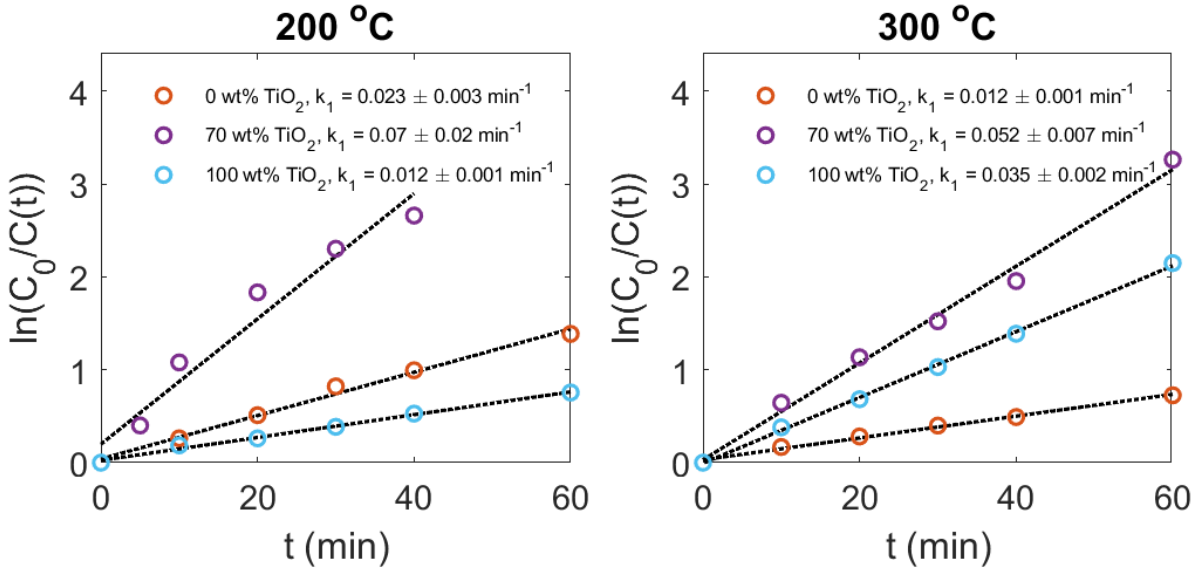

Fig. S4. Kinetics of RhB degradation in the presence of In_2O_3, TiO_2, and In_2O_3/TiO_2(70) powders annealed at 200 °C (left) and 300 °C (right). Experimental data (circles) were fitted with pseudo first-order kinetics using linear regression (dashed lines). The slopes of the linear fits, which are equal to the reaction constants (k_1), are shown in the legend, along with the amounts of TiO_2 in the samples.

3. Additional electrocatalytic data

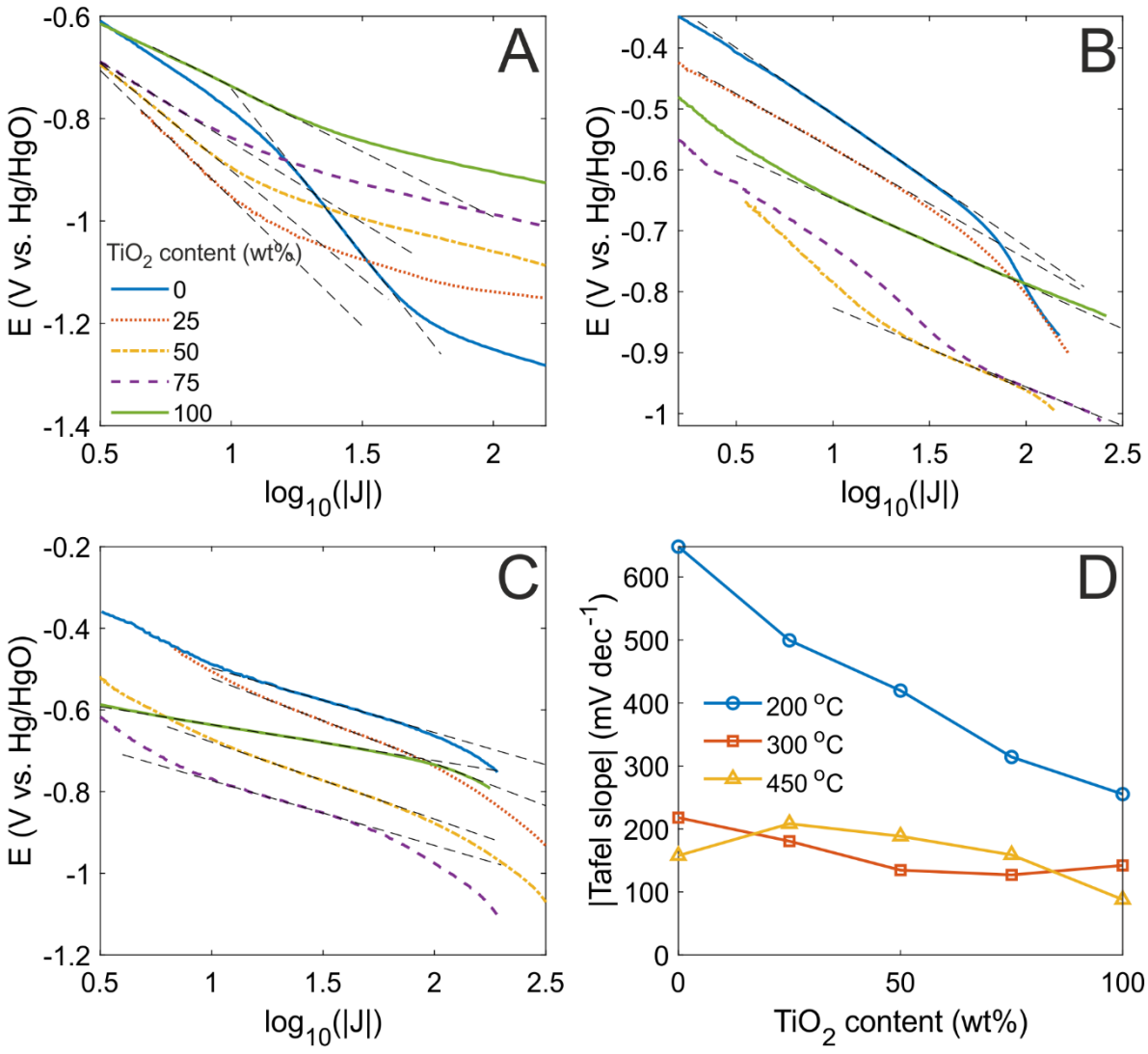

Fig. S5. Tafel plots for In_2O_3, TiO_2, and In_2O_3/TiO_2 electrodes annealed at 200 °C (A), 300 °C (B), and 450 °C (C). The legend in panel A applies to panels B and C as well. Comparison of Tafel slopes for different electrodes (D).

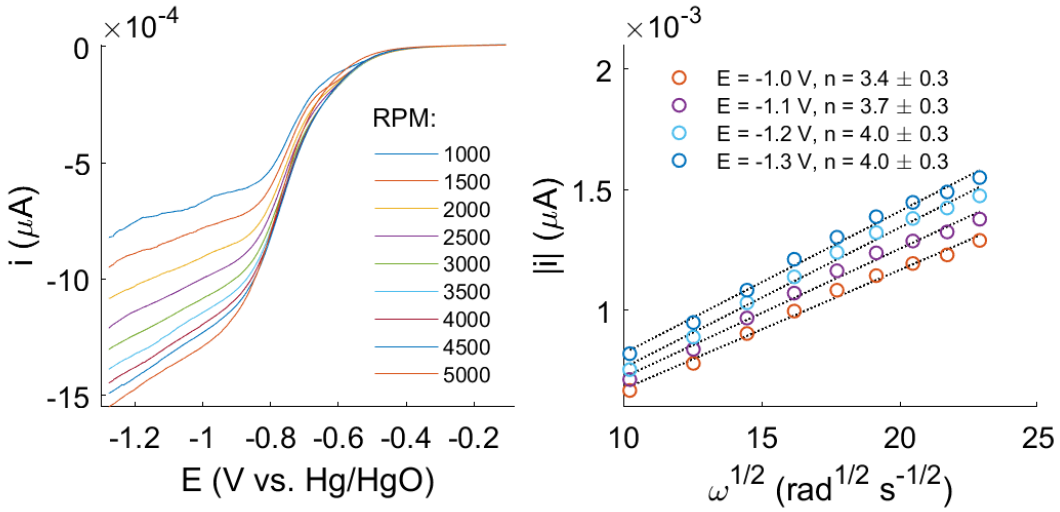

Fig. S6. Linear sweep voltammograms measured on a Ti RDE with a deposited sol-gel TiO_2 film (left), with rotational frequencies of the electrode shown in the legend. Levich plots at different potentials (right) along with the linear fits, with the corresponding numbers of electrons transferred (*n*) shown in the legend.

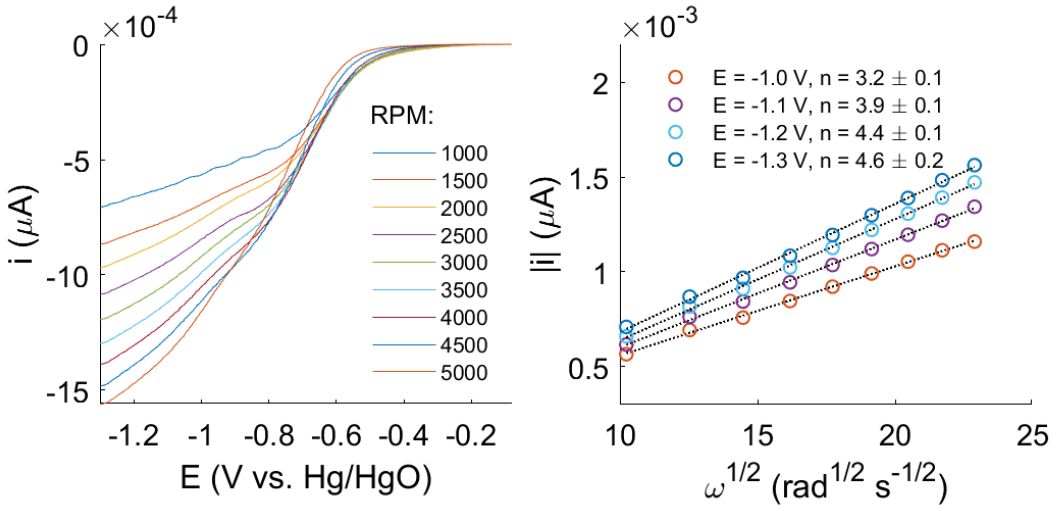

Fig. S7. Linear sweep voltammograms measured on a Ti RDE with a deposited sol-gel In_2O_3 film (left), with rotational frequencies of the electrode shown in the legend. Levich plots at different potentials (right) along with the linear fits, with the corresponding numbers of electrons transferred (*n*) shown in the legend.

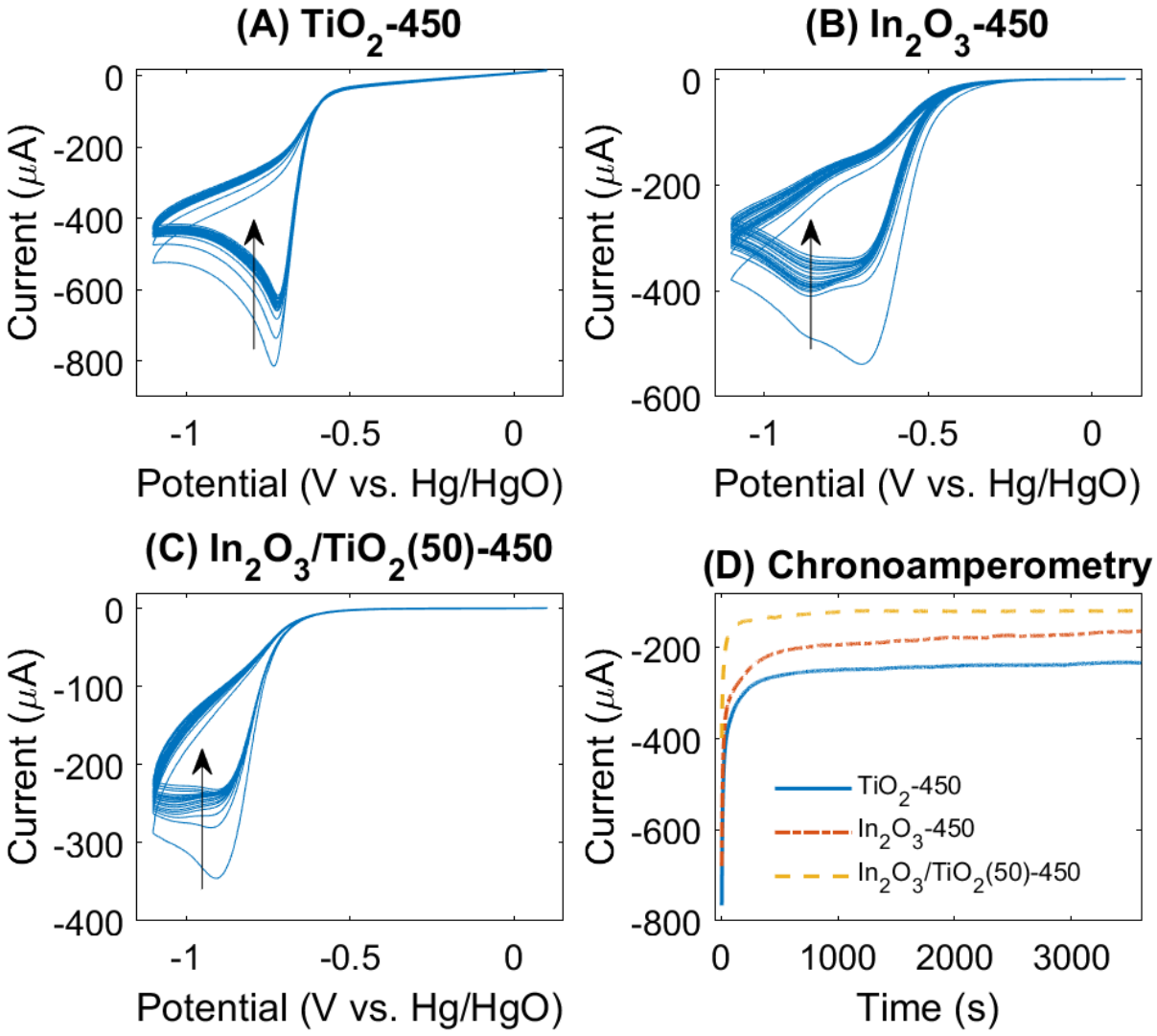

Fig. S8. Cyclic voltammograms (A–C) and potentiostatic chronoamperograms (D) for TiO_2, In_2O_3, and $In_2O_3/TiO_2(50)$ film electrodes annealed at 450 °C. Cyclic voltammograms (20 cycles) were acquired at a sweep rate of 10 mV s^{-1}. Chronoamperometry was performed at –0.8 V for the pure oxides and at –0.9 V for the composite electrode.